CORNER DETECTION WITH MINIMAL EFFORT ON MULTIPLE SCALES

Ernst D. Dickmanns
Institut für Systemdynamik und Flugmechanik, LRT, UniBw Munich, D-85577, Neubiberg, Germany
Ernst.Dickmanns@unibw.de

Keywords: Image processing, feature extraction, corner detection.

Abstract: Based on results of fitting linearly shaded blobs to rectangular image regions a new corner detector has been developed. A plane with least sum of errors squared is fit to the intensity distribution within a mask having four mask elements of same rectangular shape and size. Averaged intensity values in these mask elements allow very efficient simultaneous computation of pyramid levels and a new corner criterion at the center of the mask on these levels. The method is intended for real-time application and has thus been designed for minimal computing effort. It nicely fits into the 'Unified Blob-edge-corner Method' (UBM) developed recently. Results are given for road scenes.

1 INTRODUCTION

(Moravec, 1979) developed the first 'interest operator' for application in the field of autonomous vehicles when computing power of microprocessors was still very low. (Harris and Stephens, 1988) improved the approach by looking at local intensity gradients around the test points and by checking a local (2 x 2) 'structural matrix' *N* defined by products of gradient components. From the two eigenvalues λ of this matrix, a simple criterion for corners has been derived using $traceN = \lambda_1 + \lambda_2$ in combination with the determinant det*N*. This approach has been the ancestor of many derivatives (Tomasi and Kanade, 1991; Shi and Tomasi, 1994; Birchfield, 1994; Haralick and Shapiro, 1993) not discussed here. Methods avoiding gradient computation are favored lately (Smith and Brady, 1997; Drummond and Cipolla, 2002; Lowe 2004; Rosten and Drummond, 2004). Surveys on corner detection may be found in the bibliography (USC IRIS, Vision Bib.com, Section 6.4.4.7) and (http://users.fmrib.ox.ac.uk).

The approach presented here heavily relies on gradients for its derivation, but ends up using only four add/subtract, one division and one compare operation for stating local nonplanarity of the intensity function above a threshold ErrMax; the link of this threshold to the frequently used trace of the eigenvalues in other corner detection methods is derived. This result is achieved by looking at a correlation function between four local planar approximations and one more global one (covering the same region) as a least squares fit.

2 ROOTS OF THE NEW APPROACH

(Hofmann, 2004) has used a set of four identically sized rectangular mask elements (*mel*) for computing edges and linearly shaded intensity patches in an efficient way. This approach has been expanded in (Dickmanns, 2007) by a prior non-planarity check to separate out regions with strongly nonplanar two-dimensional distributions of intensity. Due to the basic regular mask structure (see bottom of perspective projection in Figure 1) very simple and efficiently computable results have been obtained.

The magnitude of the errors (residues) is directly proportional to the difference between the sums of the intensity values on the diagonal and the counter-diagonal, the sum of which yields the pixel intensity on the next pyramid level: (i, j = 1 or 2)

$$|\varepsilon_{ij}| = |(I_{11} + I_{22}) - (I_{12} + I_{21})| / 4 \,. \qquad (1)$$

The average intensity I_{M0} in the mask region is one quarter of the sum of these two diagonal sums (= sum of all four mask elements)

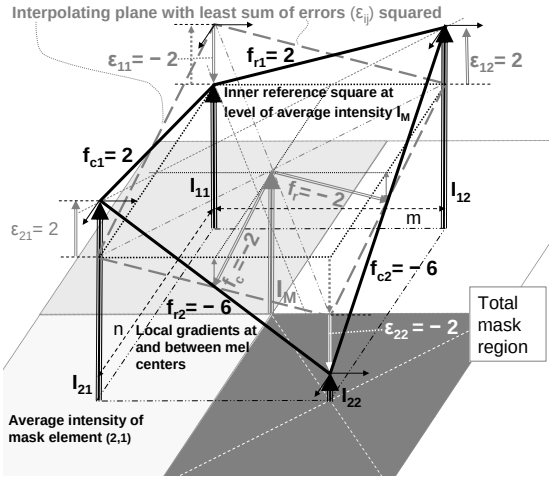

Figure 1: Basic rectangular mask structure for fitting the plane with least sum of errors squared (dashed gray lines) to the four discrete intensity values I_{ij} shown as vertical vectors. All four errors ε_{ij} are equal in magnitude and sum up to zero.

$$I_{M0} = (I_{11} + I_{12} + I_{21} + I_{22})/4. \quad (2)$$

Specifying a threshold level 'ErrMax' for this error value for separating almost planar from nonplanar intensity regions in the image allows identifying potential regions for corners in the relatively small 'nonplanar set'. As shown in (Dickmanns, 2007, Figures 5.23 and 5.26), for typical road traffic scenes this reduces the areas of interest for corner detection to only a few percent of the entire image; with 256 intensity levels in standard video images and with a gray value resolution of the human eye of around 60 levels (Darian-Smith, 1984) a threshold value around 256/60 ≈ 4 seems reasonable. Values ranging from ~ 2 to 8% (4 to 20 steps in gray value) have shown acceptable results (depending on the task).

For filtering corner candidates out of the nonplanar set, an approach similar to (Haralick, 1993) has been used, however, with a small window (size of the mask, see perspective projection in Figure 1); the (2 by 2 mel) very narrow neighborhood has its drawbacks. As a direct consequence, results obtained are susceptible to digitization noise when mask elements are chosen as original pixels. Through its principle of checking the corner conditions by diagonal sums, the method also responds to edges in the image, the orientation of which is close to diagonal. To separate real corners from (noise-corrupted) digitized edges, the method is applied again with modified parameters (see below). *TraceN* has to be above a level $traceN_{min}$ to guarantee the presence of a corner; *traceN* turns out to be proportional to the square of the error ε (Eq.(1)) in the present approach.

In most approaches derived from (Harris and Stephens, 1988), the center of the region tested for corners is a central pixel. In the approach taken in (Dickmanns, 2007), the center of the region is the point where all four mel meet; there is no direct measurement value of image intensity available at that point. Instead, the average value of mel-intensities and their gradients are adopted for this center point. Then, the question can been asked: 'How do the local intensities and their gradients at the centers of each mel correlate to the average value at the center of the mask'. This can be investigated with a correlation function. However, since with the averaged planar model for the entire mask also averaged local variations as function of y and z are available, the correlation may be refined, asking for deviations between the global and the local *planar models*. Since the methods applied for corner detection correspond to curvature determination via the Hessian matrix, *i.e.* the second derivative of the two-dimensional intensity function, the idea is enhanced, whether deviations from planar relations are not a better way to go for testing curvature. This leads to a slightly modified correlation function as compared to (Harris and Stephens, 1988); now the subtracted reference is not just the average intensity value but the *averaged planar intensity model.*

3 NEW APPROACH WITH A PLANAR REFERENCE MODEL

Figure 1 shows the four intensity values at the mel centers (heavy black vertical arrows) and the averaged intensity of the mask (gray) at the point where all mels meet. As local intensity gradients (Euler approximation) the differences between the intensities of mels in row- (f_{rj}) and column direction (f_{ci}) are chosen (solid lines). From Figure 1, the relations for the neighborhood of the mel centers are obtained:

$$\begin{aligned} I_{11L}(u,v) &= I_{11} + f_{r1}\cdot u + f_{c1}\cdot v; \\ I_{12L}(u,v) &= I_{12} + f_{r1}\cdot u + f_{c1}\cdot v; \\ I_{21L}(u,v) &= I_{21} + f_{r2}\cdot u + f_{c1}\cdot v; \\ I_{22L}(u,v) &= I_{22} + f_{r2}\cdot u + f_{c2}\cdot v; \quad \text{with} \\ f_{r1} &= (I_{12} - I_{11})/m; \quad f_{r2} = (I_{22} - I_{21})/m; \end{aligned} \quad (3)$$

$$f_{c1} = (I_{21} - I_{11})/n; \quad f_{c2} = (I_{22} - I_{12})/n.$$

The global model for the neighborhood of the mask center can be written (Dickmanns, 2007)

$$I_M(u,v) = I_{M0} + f_r \cdot u + f_c \cdot v \tag{4}$$

with $f_r = (f_{r1} + f_{r2})/2; \quad f_c = (f_{c1} + f_{c2})/2.$

The new correlation function now is

$$E(u,v) = \sum_{i,j} [I_{ijL}(u,v) - I_M(u,v)]^2 \tag{5}$$

Other than in the reference mentioned, here, absolute intensity values are used to have the same absolute intensities as thresholds for corner detection; normalizing by average intensity and using a percentage threshold favors corners in darker regions.

The term in square brackets in Eq.(5) is written for one mel-center with Eq.(3) and with the abbreviation $\Delta I_{ij} = I_{ij} - I_{M0}$

$$\begin{aligned} &\{I_{11} - I_{M0} + (f_{r1} - f_r)\cdot u + (f_{c1} - f_c)\cdot v\}^2 \\ &= \{\Delta I_{11} + 0.5\cdot[(f_{r1} - f_{r2})\cdot u + (f_{c1} - f_{c2})\cdot v]\}^2. \end{aligned} \tag{6}$$

Eq.(6) can be expanded to

$$\begin{aligned} \{\ \}^2 &= (\Delta I_{11})^2 + \Delta I_{11}\cdot[(f_{r1} - f_{r2})\cdot u + (f_{c1} - f_{c2})\cdot v] + \\ &+ [(f_{r1} - f_{r2})^2 \cdot u^2 + \\ &2\cdot(f_{r1} - f_{r2})(f_{c1} - f_{c2})\cdot u\cdot v + (f_{c1} - f_{c2})^2 \cdot v^2]\cdot 0.25. \end{aligned} \tag{7}$$

The sum S_4 of the mixed $u{\cdot}v$-terms in the center of the last row of Eq.(7) of all four intensity components (only one shown above) can be written

$$S_4 = \begin{bmatrix} (f_{r1} - f_{r2})(f_{c1} - f_{c2}) + (f_{r1} - f_{r2})(f_{c2} - f_{c1}) + \\ (f_{r2} - f_{r1})(f_{c1} - f_{c2}) + (f_{r2} - f_{r1})(f_{c2} - f_{c1}) \end{bmatrix} \cdot 2\cdot u\cdot v.$$

Summing the terms on top of each other in this equation yields zero so that the terms with the mixed factor $u{\cdot}v$ vanish in the sum of Eq.(5). This leads to a correlation function, the quadratic part of which has no cross-products. With the help of the structural matrix N this is written

$$\begin{aligned} E_{quadr}(u,v) &= \ldots + (f_{r1} - f_{r2})^2 \cdot u^2 + (f_{c1} - f_{c2})^2 \cdot v^2 \\ &= \ldots + \begin{pmatrix} u & v \end{pmatrix} \begin{pmatrix} (f_{r1} - f_{r2})^2 & 0 \\ 0 & (f_{c1} - f_{c2})^2 \end{pmatrix} \begin{pmatrix} u \\ v \end{pmatrix}. \end{aligned} \tag{8}$$

The trace is

$$traceN = (f_{r1} - f_{r2})^2 + (f_{c1} - f_{c2})^2. \tag{9}$$

From Figure 1 it can be seen that gradient f_{r1} (resp. f_{c2}) times distance m (n) between the corresponding mel-centers yields the intensity difference ($I_{12} - I_{11}$), resp. ($I_{22} - I_{12}$). Therefore, the following relation holds, relating the differences between the row gradients to those of the column gradients

$$\begin{aligned} &f_{r1}\cdot m + f_{c2}\cdot n = f_{c1}\cdot n + f_{r2}\cdot m \\ \text{or} \quad &(f_{c1} - f_{c2}) = m/n\cdot(f_{r1} - f_{r2}). \end{aligned} \tag{10}$$

For a square mask this means that the differences of gradients in row and column direction are equal. Introducing this into Eq.(9), there follows

$$traceN = (f_{r1} - f_{r2})^2 \cdot [(m/n)^2 + 1]. \tag{11}$$

This threshold criterion has thus been reduced to a simple function of the difference between local row- or column gradients, which makes sense in connection with the interpretation of the eigenvalues as measures of curvature of the intensity function. For m = n (square grid) there follows a factor of 2 in Eq.(11); *circularity* according to (Haralick, 1993) then is always $q = 1$ here.

This has been achieved by referring curvature to the special planar fit to the intensity function in the mask region with least sum of errors squared. The planarity error ε (magnitude of all residues) has already been given by Eq.(1). Introducing this and Eq.(10) into Eq.(11) finally yields *traceN* as a function of the residue value ε of the planar fit to the intensity function

$$traceN = 16\cdot\varepsilon^2 \cdot \frac{(n^2 + m^2)}{m^2 \cdot n^2}. \tag{12}$$

This is the only threshold value left for adjusting the number of corner candidates delivered by the method; for m = n = 1 (mel = pixel), the factor to the squared residue for obtaining *traceN* is 32 (Eq.(12)). To avoid the multiplications for the comparison, of course, the threshold value can be adjusted directly to ε (ErrMax). The following result is thus obtained:

All quantities necessary for corner evaluation are directly obtainable from the residue of the least squares planar fit, which in turn is nothing but the difference of two diagonal intensity sums in the mask of the method UBM.

4 EXPANSION TO MULTIPLE SCALES

Since the base for corner detection is rather small on the pixel grid, an extension to several pyramid levels is desirable. This can be achieved with little additional effort since the evaluation of the least squares planar error according to Eq. (1) already requires computation of the sums of the diagonal elements. A quarter of the sum of these diagonal sums yields the pixel intensity on the next (2 x 2) pyramid level (1 add- and 1 shift operation).

When multiple scales are used, the center of each pixel on the next scale is shifted relative to the center of the previous one (see Figure 2a). The right-hand part of the figure shows that on each pyramid level two next-higher levels have to be computed if pixel centers are to be placed on top of the previous one; fortunately, this increased computational load also saves some information from the lower level to

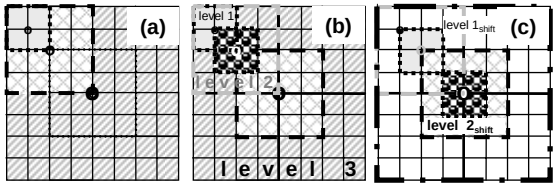

Figure 3: Computation of two images (one shifted) on next higher pyramid level is required, if centers of masks are to be positioned exactly on top of each other.

the next higher one if regions with sharp edges in row- or column direction are compared.

Figure 3 shows a standard video field with its two first pyramid levels scaled back to original size (left). The second pyramid level already looks rather blurred. The three images with the nonplanar regions found by the simple method (difference of diagonal sums larger than a threshold value) are shown on the

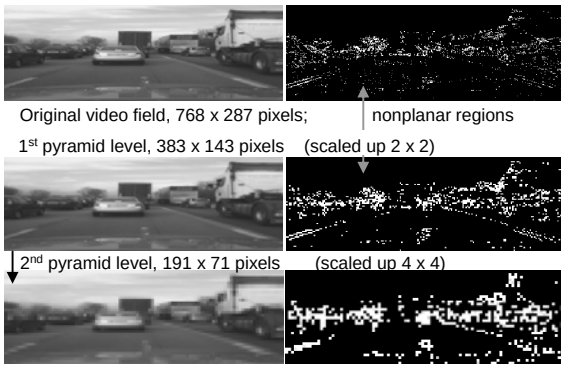

Figure 2: Original video field (top left) and two 2 x 2 pyramid images scaled to same size (left); right: candidate regions for corners found by nonplanarity tests in image intensity.

right-hand side. They allow the conclusion that pyramid level one (center) may be the best scale for detecting corners and for starting efficient recognition of objects in real-time. On level two, horizontal and vertical edges may be severely blurred, depending on the position of these edges relative to the boundaries of the pixels. Aliasing occurs at oblique edges, leading to 'artificial corners' on a local scale.

Another peculiarity to be seen from figure 3 is the fact that edges close to diagonal satisfy the simple 'diagonal test'; in order to eliminate those cases, a second test of the simple type will be applied, however, with the sensitive direction rotated by 45°. This second check needs only be applied to corner candidates from the first test (a few %).

5 A SECOND TEST WITH AXES ROTATED BY 45°

This means that now the primary gradients of intensities are chosen as diagonals in the pixel grid (see Figure 4); the diagonals are now horizontal and vertical. A measurement base of rectangular shape is used again to take advantage of the theoretical results in plane fitting. However, the gradients are now considered in diagonal direction.

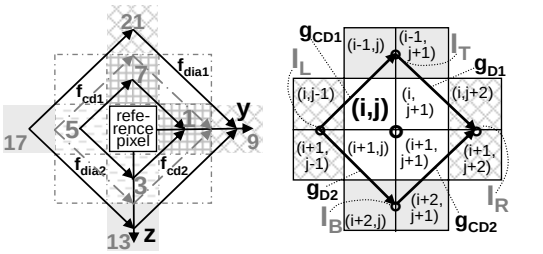

Figure 4: Rotated base (by 45°) for a second corner check using the model-based criterion from fitting a local plane to the intensity function.

With the planar model fit in rotated coordinates this leads to 'diagonal checks' which now use one or several pixels in the same columns or rows only. Several arrangements are shown. On the left, single pixels on the lowest level may be used (dark, solid arrows) or the average of two pixels in row- or column direction (dash-dotted gray arrows). For these arrangements, the origin does not coincide with the origin on the first pyramid level; the advantage is that test values are further off the original image diagonals, for which cases the simple diagonal test is not able to discriminate between edges and corners.

The case shown on the right in Figure 4 has a pixel on pyramid level 1 as center; the average of the two adjacent pixels on level 0 may be taken for the second diagonal test; however, with less effort better results are obtained by using pixels on the next higher pyramid level.

6 COMPARISON OF EFFORT NEEDED AND EXPERIMENTAL RESULTS

Beside the quality of results delivered (consistency, completeness, localization accuracy), the effort to obtain them is a criterion for general acceptance of a method. The new method has been investigated extensively with special test images and with single real-world images from video (-fields and full images). Qualitative results look promising so that a real-time implementation for video-rate is underway.

With respect to computing effort needed, Table 1 shows a comparison with other proven methods; the corner evaluation is done for every second pixel (m_r in total) in every second row (n_c in total), yielding $m_r \cdot n_c \cdot 0.25$ locations. This is considered a fair comparison to the pyramid concept in the new method. The pyramid stages are a byproduct needing just storage and only little additional computation (see Eq.(2) with a single pixel as mask element). With the size reduction by one quarter for each stage, three stages need (1 + 0.25 + 0.0625) = 1.3125 times the operations per pixel. Assuming 15% additional effort for removing corner candidates stemming from nearly diagonal edges from the first test (~ 5% of image locations and 3 times the basic effort) requires another factor of 1.15 for the total operations needed (~ 1.51 times the operations per pixel, see square brackets in last column).

Table 1: Comparison of mathematical operations needed with several corner extraction methods.

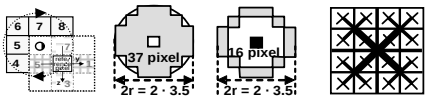

method, year	Harris, 1988	SUSAN 1997		FAST 2004	Dickmanns 2008
radius r	~ 2.5	2.5	3.5	3.5	~ 4
add/subtr.	27	28	53	22	5 [7.5]
mult./div.	13	0	0	0	1 [1.5]
compare	1	19	36	15	1 [1.5]
number of locations	$n_c \cdot m_r \cdot 0.25$	$n_c \cdot m_r \cdot 0.25$		$n_c \cdot m_r \cdot 0.25$	$n_c \cdot m_r \cdot 0.25$ [·1.51]

Since reusing intermediate results has been taken into account computing the effort needed, applying the known methods to every pixel location requires only about doubling the numbers given. For achieving the same localization accuracy, the new method would have to start from twice the image resolution, and the numbers in the last column have to be multiplied by four. This would cut the ratio between former and the last column in half, leaving still some advantage to be expected for the new method. However, since real-time visual perception runs at 25 (33⅓) Hz with smoothing by recursive estimation, this increased effort may not be necessary.

Of course, these numbers can only yield a rough estimate of computing times required by full algorithms, since hardware capabilities and programming proficiency also play an important role for the results finally achieved. Future has to show actual results.

Figure 5 shows results with two diagonal tests but without consistent pixel centering on the different pyramid levels. From the figure and many other examples investigated it has been concluded that the effort for precise superposition of mask centers may be desirable for smooth tracking in real time; an approach with two images on each higher pyramid level, one shifted by (1, 1) relative to the other (see Fig. 2), is under study and looks promising.

Note that the approach requires no computation of gradients at all. Just the sums of two pixels on the diagonal have to be computed in the framework of the fit of an intensity plane with least sum of errors squared. The difference not only yields the residues ε of the planar fit, but its square is also directly proportional to the trace of the structural matrix, *i.e.* the sum of the eigenvalues (Eq.(12)).

The use of two rotated planar fits allows lowering the threshold *traceN* for achieving detection of fainter real corners. If the threshold is set too high, candidates resulting from real corners but with low differences in intensity are lost. The second rotated planar fit eliminates, or at least strongly reduces, the number of candidates stemming from noise-corrupted edges.

For real-time applications it is not so important to detect all corners (also unreliable ones) but to obtain sufficiently many consistent candidates for tracking at high image rates. Edges are picked up by separate operators anyway. Figure 5 shows that some corner candidates are obtained on single pyramid levels only, while others are detected on two or even three levels; of course, these latter ones are those best suited for tracking.

Figure 6: Corner candidates from two rotated 'diagonal tests' on three pyramid levels (centers not adjusted): 'o' = level 0, '+' = level 1, triangles = level 2. The number of corner candidates is down to about 1/3 by the 2nd test.

7 CONCLUSIONS

The results achieved seem to support M. Planck's claimed aphorism: "There is nothing more practical than a good theory". A least squares plane fit to the averaged intensity surface in the area of four identically sized elements of a rectangular mask yields four residues of equal magnitude and opposite signs on the diagonals. By looking at the correlation between the averaged planar intensity function and the local ones at the four 'measurement points' (I_{ij}), theoretical results allow easy judgment of curvature effects based on the eigenvalues of the structural matrix with minimal computational efforts. Figure 6 visualizes the results obtained for saddle-point-like corners including the curvature effects (qualitatively), represented by the eigenvalues of the structural matrix. (Sharp intensity spikes, of course, tend to be lost by averaging; they are picked only with sufficiently high spatial resolution in the original image.)

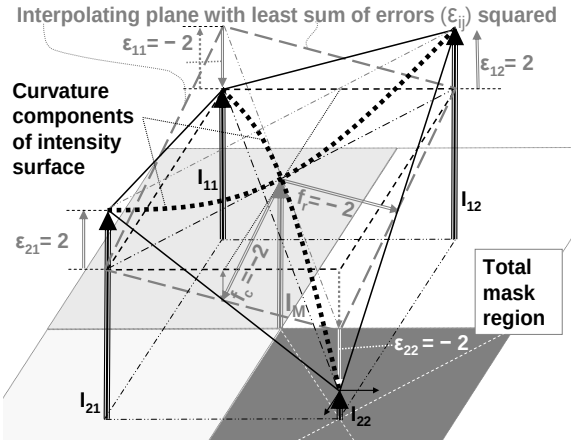

Figure 5: Visualization of the curvature components of the intensity function relative to the interpolating plane determined by the new corner detector (dotted curves).

Optimal scales (or combinations of scales) still have to be determined from image sequences with the real-time computing power actually available; the results given look promising. Through the simple nonplanarity test upfront, further corner tests may be more involved since they have to be applied to a small fraction of the image data only that passed the first test. In standard road scenes, a reduction of one to two orders of magnitude is usual.

REFERENCES

Birchfield, S., 1994. KLT: An Implementation of the Kanade-Lucas-Tomasi Feature Tracker.

Darian-Smith, I., (ed) 1984. *Handbook of Physiology*, American Physiological Society: Sensory Processes, Vol. III, Parts 1 and 2.

Dickmanns ED., 2007. *Dynamic Vision for Perception and Control of Motion*. Springer-Verlag, London.

Drummond, T., Cipolla, R., 2002. Real-time visual tracking of complex structures. *IEEE Transactions on Pattern Analysis and Machine Intelligence*, 24(7):932-946.

Harris, C., Stephens, M., 1988. A combined corner and edge detector. In: *Alvey Vision Conference*, pp 147-151.

Haralick, R.M., Shapirom L.G., 1993. *Computer and Robot Vision*. Addison-Wesley.

Hofmann, U., 2004. Zur visuellen Umfeldwahrnehmung autonomer Fahrzeuge. Diss., UniBw Munich, LRT

http://users.fmrib.ox.ac.uk
users.fmrib.ox.ac.uk/~steve/susan/susan/node11.html.

Lowe, D., 2004. Distinctive image features from scale-invariant keypoints. *International Journal of Computer Vision*, 60(2):91-l10.

Moravec, H., 1979. Visual Mapping by a Robot Rover. *Proc. IJCAI 1079*: 593-600.

Rosten, E., Drummond, T., 2004. Fusing Points and Lines for High Performance Tracking. *ICCV*, pp. 1508-1511.

Shi, J., Tomasi, C., 1994. Good Features to Track. *Proc. IEEE-Conf. CVPR*, pp. 593-600

Smith, S., Brady, J., 1997. SUSAN - a new approach to low level image processing. *International Journal of Computer Vision*, 23(l):45-78.

Tomasi, C., Kanade, T., 1991. Detection and Tracking of Point Features. *CMU, Tech. Rep. CMU-CS-91-152*, Pittsburgh, PA.

USC IRIS, Vision Bib.com. *Annotated Computer Vision Bibliography*. Section 6.4.4.7: "Corner Feature Detection Techniques and Use".